HHS Public Access

Author manuscript

Chempluschem. Author manuscript; available in PMC 2015 August 28.

Published in final edited form as:

Chempluschem. 2014 August ; 79(8): 1083–1088. doi:10.1002/cplu.201402080.

In Vivo Processing of Ceria Nanoparticles inside Liver: Impact on Free-Radical Scavenging Activity and Oxidative Stress

Dr. Uschi M. Graham[a], **Dr. Michael T. Tseng**[b], **Dr. Jacek B. Jasinski**[c], **Prof. Dr. Robert A. Yokel**[d], **Dr. Jason M. Unrine**[e], **Dr. Burtron H. Davis**[a], **Dr. Alan K. Dozier**[f], **Dr. Sarita S. Hardas**[g], **Dr. Rukhsana Sultana**[g], **Prof. Dr. Eric A. Grulke**[h], and **Prof. Dr. D. Allan Butterfield**[g]

Uschi M. Graham: graham@liquasol.com

[a]Center for Applied Energy Research and Catalysis Research and Testing Center, University of Kentucky, 2540 Research Park Drive, Lexington, KY 40511 (USA)

[b]Department of Anatomical Sciences and Neurobiology, University of Louisville, Louisville, KY 40204 (USA)

[c]Conn Center for Renewable Energy, University of Louisville, Louisville, KY 40204 (USA)

[d]Pharmaceutical Sciences and Graduate Center for Toxicology, University of Kentucky, Lexington, KY 40506 (USA)

[e]Department of Plant and Soil Sciences, University of Kentucky, Lexington, KY 40506 (USA)

[f]National Institute of Occupational Safety and Health (NIOSH), Cincinnati, OH 45226 (USA)

[g]Department of Chemistry, University of Kentucky, Lexington, KY 40506 (USA)

[h]Chemical and Materials Engineering Department, University of Kentucky, Lexington, KY 40506 (USA)

Abstract

The cytotoxicity of ceria ultimately lies in its electronic structure, which is defined by the crystal structure, composition, and size. Despite previous studies focused on ceria uptake, distribution, biopersistance, and cellular effects, little is known about its chemical and structural stability and solubility once sequestered inside the liver. Mechanisms will be presented that elucidate the in vivo transformation in the liver. In vivo processed ceria reveals a particle-size effect towards the formation of ultrafines, which represent a second generation of ceria. A measurable change in the valence reduction of the second-generation ceria can be linked to an increased free-radical scavenging potential. The in vivo processing of the ceria nanoparticles in the liver occurs in temporal relation to the brain cellular and protein clearance responses that stem from the ceria uptake. This information is critical to establish a possible link between cellular processes and the observed in vivo transformation of ceria. The temporal linkage between the reversal of the pro-oxidant effect (brain) and ceria transformation (liver) suggests a cause–effect relationship.

Correspondence to: Uschi M. Graham, graham@liquasol.com.

Supporting information for this article is available on the WWW under http://dx.doi.org/10.1002/cplu.201402080.

Keywords

biotransformations; cellular chemistry; cerium; nanoparticles; redox chemistry

Introduction

Internalized ceria nanoparticles cause distinct cellular responses that can result in both therapeutic effects[1–7] and also oxidative stress.[8–11] Oxidative stress, which can be induced in the presence of free-radical species, is considered damaging to cells, proteins, and DNA.[8,12] Nanoparticle uptake[13–16] can result in free-radical formation and exacerbate cytotoxicity when cells are under constant exposure to oxidative stress.[17] When ceria nanoparticles (CeO_2 NPs) are sequestered in a rat liver, cytotoxicity occurs, as evidenced by hepatocyte enlargement, sinusoidal dilatation, accumulation of Kupffer cells, and formation of granuloma.[18, 19] In fact, it was recently shown that CeO_2 NPs uptake by the liver also coincides with early pro-oxidant effects in the rat brain,[20] which is followed by a transition to oxidative stress and then, unexpectedly, reverses back to no stress after ninety days.[21] Despite substantial studies that have focused on CeO_2 NPs uptake, distribution, and biopersistance,[1–4,22, 23] so far, no information has been available on its chemical and structural stability once sequestered inside the liver, the organ that stores the greatest amount of CeO_2 NPs. This raises questions about possible biotransformations of CeO_2 NPs in the liver and what impact this may have on free-radical-mediated oxidative stress.

As a redox mediator, ceria can bind reactive oxygen species (ROS) such as $O_2^{\bullet -}$ and $HO^{\bullet -}$ by reversibly shifting between oxidized (Ce^{4+}) and reduced (Ce^{3+}) forms.[1–4, 8, 24] Radical-scavenging ability is significantly boosted at very small particle size.[1–4,6, 7] Moreover, the free-radical scavenging ability of CeO_2 NPs was shown to protect against ischemic stroke in an in vivo model,[2] and recently, protein-coated CeO_2 ‘nano-truffle’ NPs were shown to have excellent redox enzyme activity that resulted in enhanced free-radical scavenging.[1–3] Therefore, it is important to determine the mechanisms that govern cellular responses and the role CeO_2 NPs play. Herein, we report for the first time that intravenously administered CeO_2 NPs after ninety days undergo in vivo processing inside the rat liver causing a shift towards smaller particle size and increased reactive surface area. Detailed analyses of the redox activity of the in vivo processed ceria nanoparticles are presented.

Results and Discussion

Nanoceria

The original intravenously administered CeO_2 NPs were cubes with (100) crystal faces (see Figure 1 and Figure S1 in the Supporting Information) and a size range of approximately (31±4) nm as determined by dynamic light scattering, and were synthesized by means of a hydrothermal precipitation method, filtered, sterilized, and sonically redispersed in aqueous solution with a citrate capping agent to obtain a 5% ceria aqueous dispersion, which was then intravenously (iv) infused into male Sprague Dawley rats (Figure S2; 85 mg kg^{-1}).[24] The high dose is well outside the previously determined therapeutic window for ceria in

vivo[3] and was mainly used because of our previous study that was centered on characterizing the safety and toxicity of nanoceria.[22–24] Details of CeO_2 NPs distribution, clearance, and biopersistance are described elsewhere.[22, 23] Liver-tissue sections were scanned for the occurrence of CeO_2 NPs and any tissue alterations that resulted after ninety days (Figure S2, which shows light microscopy and Figures S3, S5, and S6 for transition electron microscopy (TEM)). The CeO_2 NPs formed agglomerates in the liver up to day thirty, but otherwise showed no indication of breakdown or chemical transformation.[18, 19,21] However, after ninety days inside the liver, the iv-infused cube-shaped CeO_2 NPs (Figure 1a) had become highly fragmented and rounded along their edges (Figure 1b), which indicated that in vivo processing of the particles had occurred. Moreover, accumulations of copious ultrafine (1–3 nm) crystallites that formed in the liver within close proximity to the rounded CeO_2 NPs were discovered for the first time and labeled as CeO_2 clouds (Figure 1c, d). These second-generation ceria particles (crystallites in CeO_2 clouds) seem to be trapped in ‘groups or swarms’ owing to fast precipitation, which favors the formation of the CeO_2 clouds near the vicinity of the parent particles, and there is clearly an analogy with the formation of other oxide nanoparticles seen in human lung fibroblasts.[25]

The CeO_2 clouds consist of discrete 1–3 nm CeO_2 NPs with a cross-lattice pattern (Figure 1d). Corresponding electron-diffraction ring patterns (selected-area electron diffraction (SAED)) were used in conjunction with known diffraction patterns from CeO_2 as a fingerprint for phase identification of the CeO_2 clouds (PCED2.0), which revealed dominant (111), (200), and (311) faces that are not prominently seen with the as-synthesized cubes (Figure 1d). Polycrystalline large CeO_2-grains after Ostwald ripening were also observed (Figure S3). The hydrothermally derived ceria used in the iv infusions represent a group rather than all types of ceria used in industry today and the in vivo performance of industrially significant ceria from commercial applications (typically high-temperature processes, that is, combustion[26]) may be different from those of the current hydrothermal ceria and, therefore, also need to be systematically investigated. Such studies will help to get a clearer understanding of the roles that nanostructures play after particle exposure and uptake.[26] The hydrothermal ceria were chosen because of their narrow size range and cube shape to be more easily recognizable in vivo.

Redox potential of second-generation nanoceria formed inside the liver

For the first time, ceria is shown to undergo a size transformation inside the liver as demonstrated by the formation of very small 1–3 nm CeO_2 NPs, and at such a small scale ceria is well known to have therapeutic activity in free-radical reduction.[1, 2, 5–7] Briefly, the autocatalytic ability of ceria to shift between Ce^{4+} and Ce^{3+} in the crystal lattice relies on the concentration of surface defects or oxygen vacancies in the outer surface layer of crystals,[27] and, in the case of ultrafines, the entire crystallites will have defects (CeO_{2-x}) that may further augment the reducing activity of the CeO_{2-x} NPs.[28] Particles smaller than 4 nm were found previously to be completely reduced to $CeO_{1.5}$ NPs and have a fluorite structure that is essentially the same as that of CeO_2 NPs.[27, 28] In other words, the valence of Ce ions in ultrafine CeO_{2-x} NPs is a function of their particle size.[27, 28] The redox potential of CeO_{2-x} NPs both after hydrothermal synthesis and after in vivo processing in the liver was assessed with electron energy-loss spectroscopy (EELS, see Figure S4). EELS

measurements with great spatial resolution (nanoprobe ≈0.15 nm; collection angle, 30 mrad) in high-resolution scanning mode (scanning transmission electron microscopy (STEM)) allowed for specific nanoparticles to be analyzed (Figure 2). Only short electron-beam irradiation was allowed to avoid thermal damage that has been shown to alter the valence of Ce ions from Ce^{4+} to Ce^{3+} caused by loss of oxygen from the crystal lattice.[27] To analyze the valence of Ce, EELS spectra containing the Ce $M_{4,5}$-edge with information on the spin–orbital 4f occupancy (M_4 edge at 901 eV ($3d_{3/2} \rightarrow 4f_{5/2}$) and M_5 edge at 893 eV ($3d_{5/2} \rightarrow 4f_{7/2}$)) were obtained as a relative measure of CeO_{2-x} NPs valence states.[27, 28] The ratios in M_5/M_4 line edges are used to obtain the valence of cerium ions and the intensity of the M_4 edge is higher than that of M_5 when Ce^{4+} is dominant, whereas the reverse occurs when Ce^{3+} is dominant. Spectra were taken from the edge (surface region) and the core of larger particles to obtain Ce^{3+}/Ce^{4+} ratios. Both synthesized CeO_2 NPs (Figure 2a) and those that had undergone in vivo processing (rounding) in the liver (Figure 2b) were analyzed. For the in vivo rounded grains we first visually identified particles that were significantly affected during the biotransformation and then examined the local redox variations within single grains (Figure 2b, c, d). For the very small 1–3 nm crystallites in CeO_2 clouds we could only obtain a Ce^{3+}/Ce^{4+} ratio for the whole particle (Figure 2d). The representative Ce $M_{4,5}$-edge spectra for the freshly synthesized cubes (Figure 2a) and in vivo rounded grains (Figure 2b) included both surface and core analyses. The core region of both fresh and in vivo processed grains always showed characteristic satellite peaks (Figure 2a, b), which suggests a highly equilibrated content of Ce^{4+} while the surfaces of the same particles are high in Ce^{3+}. This is in good agreement with a previous study for Ce^{3+}/Ce^{4+} variations in nanoceria.[28–31] All CeO_2 surfaces in this study had M_5/M_4 ratios ranging between 1.1 and 1.4, and the core regions averaged approximately 0.9 for the cubes (Figure 2c) and approximately 0.92 for the in vivo processed grains (Figure 2d), which is close to equilibrated ceria. The M_5/M_4 ratio was computed by fitting Gaussians to the M_5 and M_4 peaks and computing the Gaussian amplitude ratios. Figure 2c, d display the computed M_5/M_4 ratio plots for representative EELS profiles that were acquired by analyzing nanoparticle cross-sections before (Figure 2c) and after (Figure 2d) in vivo processing. A significant enrichment in Ce^{3+} is always observed in surface layers whereas the core regions are primarily Ce^{4+} (reduction potential of as-synthesized ceria cubes and that of processed rounded grains in the liver are essentially the same). However, EELS analyses of ultrafines (≈ 1–3 nm) from CeO_2 clouds had much weaker M_4 lines and lacked satellite peaks (Figure 2e). Figure 2e shows representative M_5 and M_4 lines for 1, 2, and 3 nm particles from the CeO_2 clouds that indicate a reduced valence (Ce^{3+}) state for the entire grains (particles were too small for line profiles). A total of fifty crystallites had a range from 38 to 70 % Ce^{3+}, which indicates that CeO_2 cloud formation shifts the overall redox activity of ceria to a more reduced state and, thus, higher free-radical scavenging activity. The increase in oxygen vacancies in the crystal lattice of CeO_2 cloud particles is also demonstrated by variations in the oxygen K-edge (Figure S4).

In vivo processing mechanisms of nanoceria

A mechanism for the in vivo processing and rounding of the iv-infused CeO_2 NPs could be a partial dissolution of high-energy edge sites. So far, dissolution rates of CeO_2 thin films have been measured for various acidic[32] (i.e., HCl and H_2SO_4) and oxidizing (addition of

H_2O_2)[32] media, despite common views that CeO_2 is a highly insoluble refractory oxide.[33] Furthermore, uptake and biotransformation of CeO_2 NPs in a recent cucumber-plant system led to Ce phosphate rods in intercellular spaces.[34] We also show formation of rod-shaped crystallites in the liver near in vivo processed CeO_2 NPs; they are composed of Ce, O, and P as shown in TEM and corresponding energy-dispersive X-ray spectroscopy (EDS) analyses (Figure 1e; Figure S5) and are of comparable size and morphology as sol–gel-derived Ce phosphates.[35] Since significantly more CeO_2 clouds formed in the liver than in the spleen (even though the spleen had sequestered approximately the same amount of CeO_2 NPs (Figure S6)), it is possible that the liver environment promotes the processing of CeO_2 NPs through its localized liver acid–base physiology (cellular pH is tightly regulated and the CeO_2 NPs would primarily encounter a low pH in lysosomes). Oxidation of carbohydrates and fat typically results in H^+ and HCO_3^- production, which can feasibly affect partial dissolution of sequestered CeO_2 NPs based on earlier solubility studies.[32, 34,35] The in situ formation of CeO_2 clouds, therefore, could be governed by the release of Ce ions derived from dissolving iv-infused ceria in the liver since the ceria dissolution rate is a function of local pH and electrochemical potential.[32] Many ceria catalyst investigations have convincingly established the surface reduction of small ceria particles during, for example, water–gas shift (WGS) reactions[36] and in one view[37] CeO_2 NPs with high Ce^{3+} surface concentration may be oxidized leading to a metastable Ce^{4+} complex [see the Supporting Information; Eqs. (1)–(3) are an extension of redox reactions observed during WGS catalysis of ceria]. ROS, particularly hydroxyl radicals ($OH^{\bullet}$), can react with surface geminal hydroxides of the high-energy CeO_2-edge sites, which could release an $[O=CeO_2H]^{\bullet}$ radical and additional water. To form monomer Ce oxyhydroxide ($O=Ce(OH)_2$), the released $[O=CeO_2H]^{\bullet}$ radical would have to react with a hydrogen radical and the monomer Ce oxyhydroxide could then oligomerize to the intermediate dimer, followed by oligomerization to higher-molecular-weight seed nuclei (and then nanoparticles in clouds) and additional free water [see the Supporting Information; Eqs. (4)–(6)]. In vivo processing leads to a much greater reactive ceria surface area in the second-generation ceria (CeO_2 clouds). EELS of the cloud particles demonstrated that the oxidation state, when compared with the original ceria, is more reduced and we suggest that in vivo processing is a function of 1) the acidic environment, 2) the oxidizing potential of the environment, and 3) the exposure time (it took ninety days before the effects of in vivo processing were recognized in tissue samples).

At this point it is important to better understand the oxygen-tuning capability of ultrafines in the liver (second-generation ceria). We set out to determine how fast the second-generation ceria, after exposure to an oxidant (ceria acts like an oxygen scrubber), would be able to return back to the reduced state ($Ce^{4+} \rightarrow Ce^{3+}$), since EELS demonstrated that all particles in the second-generation ceria clouds were in a reduced state. An earlier study on synthesized ceria focused on the oxidation ($Ce^{3+} \rightarrow Ce^{4+}$) of ultrafines and used high-resolution X-ray photoelectron spectroscopy (XPS) to evaluate the redox state before and after incubation of the nanoparticles with hydrogen peroxide.[38] Since XPS could not be performed directly on CeO_2 clouds because nanoparticles cannot be isolated because of strong liver tissue interactions, we synthesized 2–4 nm CeO_2 NPs to resemble the crystallites in CeO_2 clouds (Figure 1b, f). To mimic the redox activity of the CeO_2 clouds we first followed previously

reported oxidation experiments[38] (using 0.5 M H_2O_2 that quickly evaporated) and oxidized the particles. The Ce^{3+}/Ce^{4+} ratios and concentration of Ce^{3+} were determined using integrated peak areas. (PAS energy of 50 eV: six peaks associated with Ce^{4+} (binding energy (BE) at 882.1, 888.0, 898.1, 900.9, 906.3, and 916.3 eV) and four with Ce^{3+} (BE at 880.2, 886. 0, 903.2, and 905.0 eV) were used for the deconvolution). Immediately after oxidation, the XPS spectrum had no peaks associated with Ce^{3+} (Figure 3), which is consistent with previous studies that showed ultrafine ceria convert the maximum amount of oxygen into available oxygen vacancies in the ceria lattice in the presence of an external oxidant.[38] We observed that the 2–4 nm ceria had approximately 40 % Ce^{3+} before H_2O_2 exposure and approximately 0 % Ce^{3+} afterwards, and furthermore in less than 1 h transitioned back to the pre-H_2O_2 baseline composition (Figure 3). Our study shows that oxidized ultrafine ceria return quickly and completely to the reduced state without the presence of reducing agents (Figure 3). The in vivo transformation and reducing potential of ultrafine CeO_2 in the liver is shown in the predictive model in Figure 4, which suggests four key steps including: 1) nanoparticle sequestration in a complex acid–base-controlled environment (liver) with some dissolution of original particles; 2) in situ formation of second-generation ceria (CeO_2 clouds); 3) greater reactive surface area for the second-generation ceria inside CeO_2 clouds; and 4) higher Ce^{3+} associated with second-generation ceria. We propose that the in vivo transformation of ceria is a dynamic system (Figure S7).

Our earlier reported results on the brain cellular responses that stemmed from the uptake of CeO_2 NPs by the liver,[21] and occurred in the same experimental system as the current study, were included in the predictive model (Figure 4). The model establishes a temporal link between cellular processes in the brain[21] and the in vivo transformation of ceria in the liver. Prior to in vivo processing of ceria, oxidative stress gradually increased in ceria-treated rats and brain cellular stress (stage S1; 1 h–1 d; antioxidant defense) was then followed by brain inflammation (stage S2; 1–7 d; pro-inflammatory response) and then brain-cell death (stage S3; 7–30 days; mitochondrial-mediated cytotoxic effects).[21] There is an analogy with a published hierarchical model,[9] however, after ninety days an unexpected brain cellular clearance response was reported,[21] which is shown in the model at stage S4 (30–90 days) and indicates a reversal or decrease in oxidative stress.[21] The model also includes the index of cellular redox status that was obtained from the ratio of oxidized glutathione (GSSG) to reduced glutathione (GSH);[21] reduced GSH constitutes approximately 98 % of cellular GSH in the absence of cellular stress and GSSG/GSH typically increases under conditions in which cellular redox potential in pathological tissues is compromised.[39] Brain oxidative stress is shown to have increased as early as one hour after CeO_2 NPs infusion (signaling pathway: Nrf-2), and one day later triggered brain inflammation (signaling pathway: TNFα (NF-kB IL-1b)).[21] The model also shows that between seven and thirty days, inflammation is significantly increased in the hippocampus, cortex, and cerebellum, and brain-cell death occurs at thirty days (signaling pathway: pro-apoptotic; Pro-Caspase-3), and then followed by autophagy (LC-3AB), and finally returns to normal levels at ninety days.[21] Importantly, the late cellular and protein-clearance response previously observed in the rat brain[21] coincides with the inception of in vivo processing of CeO_2 NPs as shown in the predictive model (Figure 4). Since the processed nanoparticles in the liver (second-generation ceria) were shown to have high Ce^{3+}, they may also have a high

affinity for reactive oxygen species and free-radical scavenging activity. Although the mechanisms are not established at this time, it could be anticipated that the in vivo processing of ceria has far-reaching protective effects, as was observed with the reversal in pro-oxidant brain effects.[2, 21]

Conclusion

In conclusion, we have demonstrated that iv-infused ceria nanoparticles, after prolonged residence time in the liver (90 days), undergo in vivo processing. This transformation includes a particle-size effect towards ultrafines (second-generation ceria), combined with a measurable change in the valence reduction and redox activity that can be linked to the free-radical scavenging activity of ceria in a previous study.[1–7,21] This is the first record to show that ceria undergoes partial dissolution inside the liver and the consequences of this are far-reaching since cerium ions presumably can be more mobile than nanoparticles and also have different cytotoxicity effects.[40–42] It will be important to determine the transport properties of released cerium ions and the potential precipitation mechanisms or any other mechanisms that lead to the second-generation ceria both interior and exterior of the liver. This information will be critical to establish a direct linkage between cellular processes like the reversal in pro-oxidative stress in the brain[21] and in vivo processing and transformation of ceria. The fact that the second-generation ceria were found as very small particles grouped together in clouds or swarms suggests some type of in vivo controlled surface functionalization.[1, 3, 17, 43–45] The long-term ceria in vivo effects may be described as a dynamic system that alters and redistributes ceria. This could be a step towards improving ceria biocompatibility in vivo.

Experimental Section

All experimental conditions, sample preparation, and analysis procedures are listed in detail in the Supporting Information. This includes material and synthesis procedures for ceria; hydrothermal synthesis conditions and nanoparticle-coatings preparations; characterization of Ce concentrations and dispersion using inductively coupled plasma mass spectrometry (ICP-MS) analysis; light microscopy of ceria and tracking the nanoparticles in liver tissue; high-resolution TEM and STEM imaging and EELS analysis of the CeO_2 NPs; and XPS analyses. A detailed description of the animal care, ceria infusion into rats, animal termination and tissue harvesting, and histopathology analysis is also included with information on how the distribution of CeO_2 NPs in organs was obtained.

Supplementary Material

Refer to Web version on PubMed Central for supplementary material.

Acknowledgments

The U.S. Environmental Protection Agency (EPA) is acknowledged for providing financial support (EPA Science to Achieve Results (STAR) Grant RD-833772 and Mr. Matt Hazzard for graphical design)

References

1. Liu X, Wei W, Yuan Q, Zhang X, Li N, Du Y, Ma G, Yan C, Ma D. Chem Commun. 2012; 48:3155.
2. Kim CK, Kim T, Choi IY, Soh M, Kim D, Kim YJ, Jang H, Yang HS, Kim JY, Park HK, Park S, Yu T, Yoon BW, Lee SH, Hyeon T. Angew Chem. 2012; 124:11201;.Angew Chem Int Ed. 2012; 51:11039.
3. Pirmohamed T, Dowding JM, Singh S, Wasserman B, Heckert E, Karakoti AS, King JES, Seal S, Self WT. Chem Commun. 2010; 46:2736.
4. Celardo I, Pedersen JZ, Traversa E, Ghibelli L. Nanoscale. 2011; 3:1411. [PubMed: 21369578]
5. Karakoti AS, Monteiro-Riviere NA, Aggarwal R, Davis JP, Narayan RJ, Self WT, McGinnis J, Seal S. JOM. 2008; 60:33. [PubMed: 20617106]
6. Korsvik C, Patil S, Seal S, Self WT. Chem Commun. 2007:1056.
7. Giri S, Karakoti A, Graham RP, Maguire JL, Reilly CM, Seal S, Rattan R, Shridhar V. PLOS. 2013; 8:e54578.
8. Lee YH, Cheng FY, Chiu HW, Tsai JC, Chen CY, Wang YJ. J Biomat. 2014; 35:4706.
9. Li N, Xia T, Nel AE. Free Radical Biol Med. 2008; 44:1689. [PubMed: 18313407]
10. Shekunova TO, Ivanova OS, Baranchikov AE, Ivanov VK, Shcherbakov AB. Nanomed: Nanotech Biol Med. 2012; 1:2.
11. Yokel RA, Florence RL, Unrine JM, Tseng MT, Graham UM, Wu P, Grulke EA, Sultana R, Hardas SS, Butterfield DA. Nanotoxicology. 2009; 3:234.
12. Willis J, Patel Y, Lentz BL, Yan S. Proc Natl Acad Sci USA. 2013; 110:10592. [PubMed: 23754435]
13. Gao H, Yang Z, Zhang S, Cao S, Shen S, Pang Z, Jiang X. Sci Rep. 2013; 3:2534. [PubMed: 23982586]
14. Patil S, Sandberg A, Heckert E, Self W, Seal S. Biomaterials. 2007; 28:4600. [PubMed: 17675227]
15. Karakoti AS, Singh S, Kumar A, Malinska M, Kuchibhatla SVNT, Wozniak K, Self WT, Seal S. J Am Chem Soc. 2009; 131:14144. [PubMed: 19769392]
16. Kim JA, Åberg C, Salvati A, Dawson KA. Nat Nanotechnol. 2012; 7:62. [PubMed: 22056728]
17. Rancan F, Nazemi B, Rautenberg S, Ryll M, Hadam S, Gao Q, Hackbarth S, Haag SF, Graf C, Rühl E, Blume-Peytavi U, Lademann J, Vogt A, Meinke MC. Skin Res Technol. 2014; 20:182. [PubMed: 24033792]
18. Tseng MT, Lu X, Duan X, Hardas SS, Sultana R, Wu P, Unrine JM, Graham UM, Butterfield DA, Grulke EA, Yokel RA. Toxicol Appl Pharmacol. 2012; 260:173. [PubMed: 22373796]
19. Tseng MT, Fu Q, Lor K, Fernandez-Botron GR, Deng Z-B, Graham U, Butterfield DA, Grulke EA, Yokel RA. Toxicologic Pathology. 10.1177/0192623313505780
20. Hardas SS, Butterfield DA, Sultana R, Tseng MT, Dan M, Florence RL, Unrine JM, Graham UM, Wu P, Grulke EA, Yokel RA. Toxicol Sci. 2010; 116:562. [PubMed: 20457660]
21. Hardas SS, Sultana R, Warrier G, Dan M, Wu P, Grulke EA, Tseng MT, Unrine JM, Graham UM, Yokel RA, Butterfield DA. Nanotoxicology. 10.3109/17435390.2013.868059
22. Yokel RA, Au TC, MacPhail RC, Hardas SS, Butterfield DA, Sultana R, Goodman M, Tseng MT, Dan M, Haghnazar H, Unrine JM, Graham UM, Wu P, Grulke EA. Toxicol Sci. 2012; 127:256. [PubMed: 22367688]
23. Yokel RA, Tseng MT, Dan M, Unrine JM, Graham UM, Wu P, Grulke EA. Nanomed: Nanotech Biol Med. 2013; 9:398.
24. Mai HX, Sun LD, Zhang YW, Si R, Feng W, Zhang HP, Liu HC, Yan CH. J Phys Chem B. 2005; 109:24380. [PubMed: 16375438]
25. Limbach LK, Li Y, Grass RN, Brunner TJ, Hintermann MA, Muller M, Gunther D, Stark WJ. Environ Sci Technol. 2005; 39:9370. [PubMed: 16382966]
26. Walser T, Limbach LK, Brogioli R, Erismann E, Flamigni L, Hattendorf B, Juchli M, Krumeich F, Ludwig C, Prikopsky K, Rossier M, Saner D, Sigg A, Hellweg S, Gunther D, Stark WJ. Nat Nanotechnol. 2012; 7:520. [PubMed: 22609690]

27. Wu L, Wiesmann HJ, Moodenbaugh AR, Klie RF, Zhu Y, Welch DO, Suenaga M. Phys Rev B. 2004; 69:125415.
28. Paier J, Penschke C, Sauer J. Chem Rev. 2013; 113:3949. [PubMed: 23651311]
29. Deshpande S, Patil S, Kuchibhatla S, Seal S. Appl Phys Lett. 2005; 87:133113.
30. Haigh SJ, Young NP, Sawada H, Takayanagi K, Kirkland AI. Micros Microanal. 2011; 17:1592.
31. Turner S, Lazar S, Freitag B, Egoavil R, Verbeeck J, Put S, Strauven Y, Van Tendeloo G. Nanoscale. 2011; 3:3385. [PubMed: 21720618]
32. O'Neill, J.; Petrov, P.; Skinner, SJ.; Ryan, MP.; Lee, WE. 10 Conference, Decommissioning, Immobilisation and Management of Nuclear Waste for Disposal; Manchester, UK. 2010;
33. Tamilmani S, Lowalekar V, Raghavan S, Small R. Solid State Phenomena. 2005; 103:283.
34. Zhang P, Ma Y, Zhang Z, He X, Zhang J, Guo Z, Tai R, Zhao Y, Chai Z. ACS Nano. 2012; 6:9943. [PubMed: 23098040]
35. Rajesh K, Mukundan P, Pillai PK, Nair VR, Warrier KGK. Chem Mater. 2004; 16:2700.
36. Gorte RJ, Zhao S. J Catalysis Today. 2005; 104:18.
37. Samuni A, Czapski G. J Chem Soc Dalton Trans. 1973:487.
38. Zhang J, Ju X, Wu ZY, Li T, Hu TD, Xie YN, Zhang ZL. Chem Mater. 2001; 13:4192.
39. Owen JB, Butterfield DA. Meth Molec Bio. 2010; 648:269.
40. Stark WJ. Angew Chem. 2011; 123:1276.Angew Chem Int Ed. 2011; 50:1242.
41. Karakoti AS, Das S, Thevuthasan S, Seal S. Angew Chem. 2011; 123:2024.Angew Chem Int Ed. 2011; 50:1980.
42. Sameer D, Swanand P, Satyanarayana VNTK, Seal S. Appl Phys Lett. 2005; 87:133113.
43. Das M, Patil S, Bhargava N, Kang JF, Riedel LM, Seal S, Hickman JJ. Biomaterials. 2007; 28:1918. [PubMed: 17222903]
44. He X, Zhang H, Ma Y, Bai W, Zhang Z, Lu K, Ding Y, Zhao Y, Chai Z. Nanotechnology. 2010; 21:285103. [PubMed: 20562477]
45. Chang JS, Chang KL, Hwang DF, Kong ZL. Environ Sci Technol. 2007; 41:2064. [PubMed: 17410806]

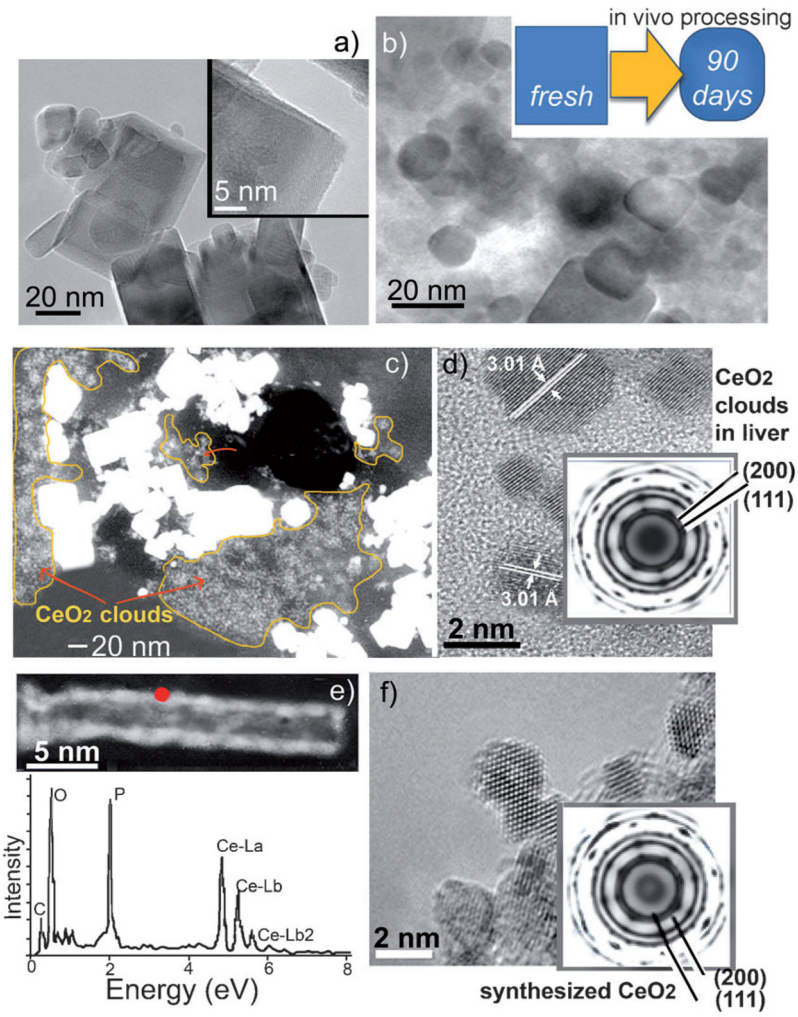

Figure 1.

HRTEM images of the ceria nanoparticles: (a) as-synthesized CeO_2 NPs with (100) faces and (b) rounded CeO_2 NPs after in vivo processing in liver; (c) STEM image of a liver section with CeO_2 NPs and ultrafine CeO_2 clouds (inside yellow line); (d) HRTEM image: ultrafine crystallites from CeO_2 clouds; the inset shows electron-diffraction rings with dominant (111) and (200) faces, which indicate that particles in the clouds are well crystallized; (e) STEM image of rod-shaped crystals; the inset is the EDS analysis with Ce-O-P composition; (f) HRTEM image: synthesized 2–4 nm CeO_2 crystallites; the inset shows that the electron-diffraction rings are the same as those of the CeO_2 clouds in (d).

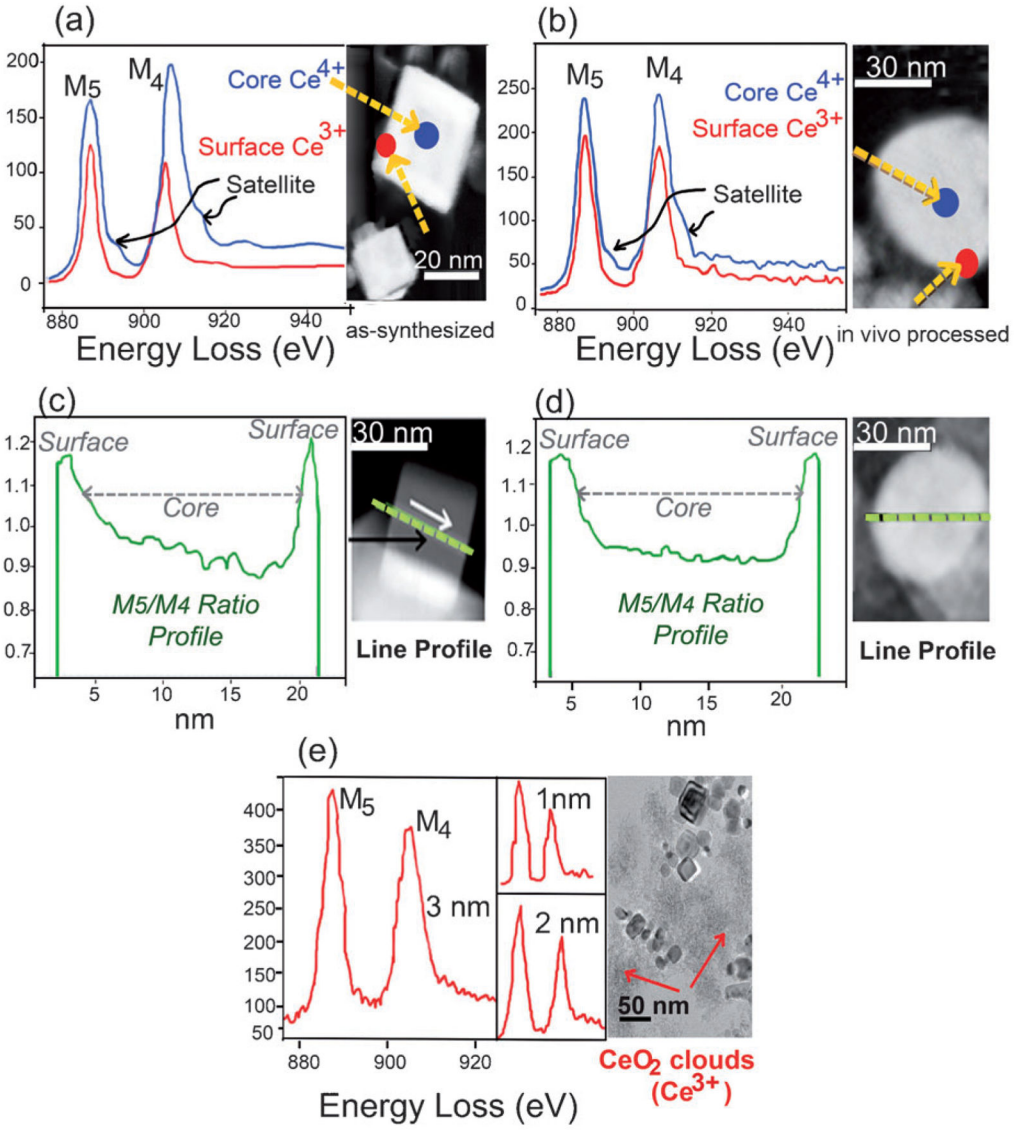

Figure 2.

EELS analysis of CeO_2 NPs: (a) the as-synthesized CeO_2 cubes; (b) in vivo processed ceria after 90 d in the liver; (c) M_5/M_4 ratio from the line profile of as-synthesized CeO_2 NPs; (d) M_5/M_4 ratio from the line profile of rounded in vivo processed CeO_2 NPs; (e) representative M_4 and M_5 lines for individual 1, 2, and 3 nm crystallites (in CeO_2 clouds. which indicate enhanced +3 reduction as a function of particle size.

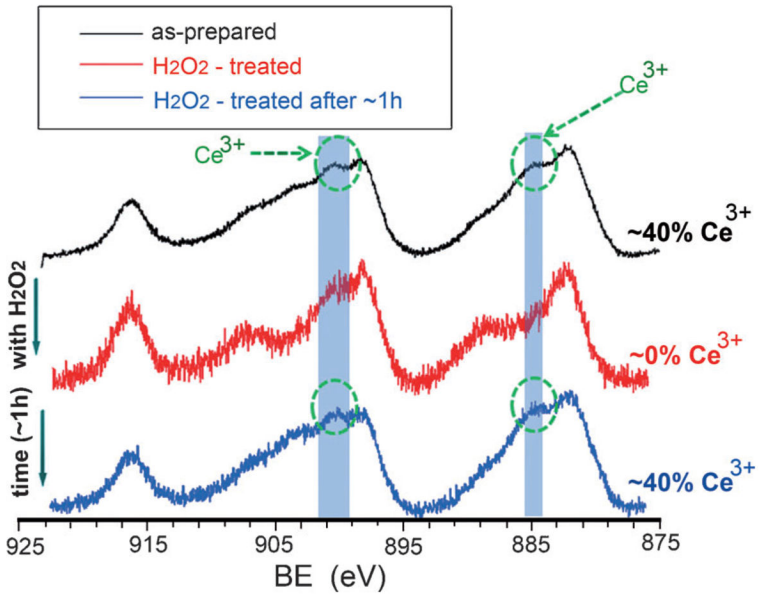

Figure 3.

XPS spectra of synthesized ultrafine CeO_2 NPs: (a) high-resolution Ce(3d) spectra of ultrafine (2–4 nm) synthesized CeO_2 NPs at three different stages: as-prepared (≈ 40 % Ce^{3+}), after oxidation with H_2O_2 (≈ 0% Ce^{3+}), and after 1 h elapsed past oxidation with H_2O_2 (≈ 40 % Ce^{3+}). As-prepared and H_2O_2-treated samples after approximately 1 h show identical survey spectra.

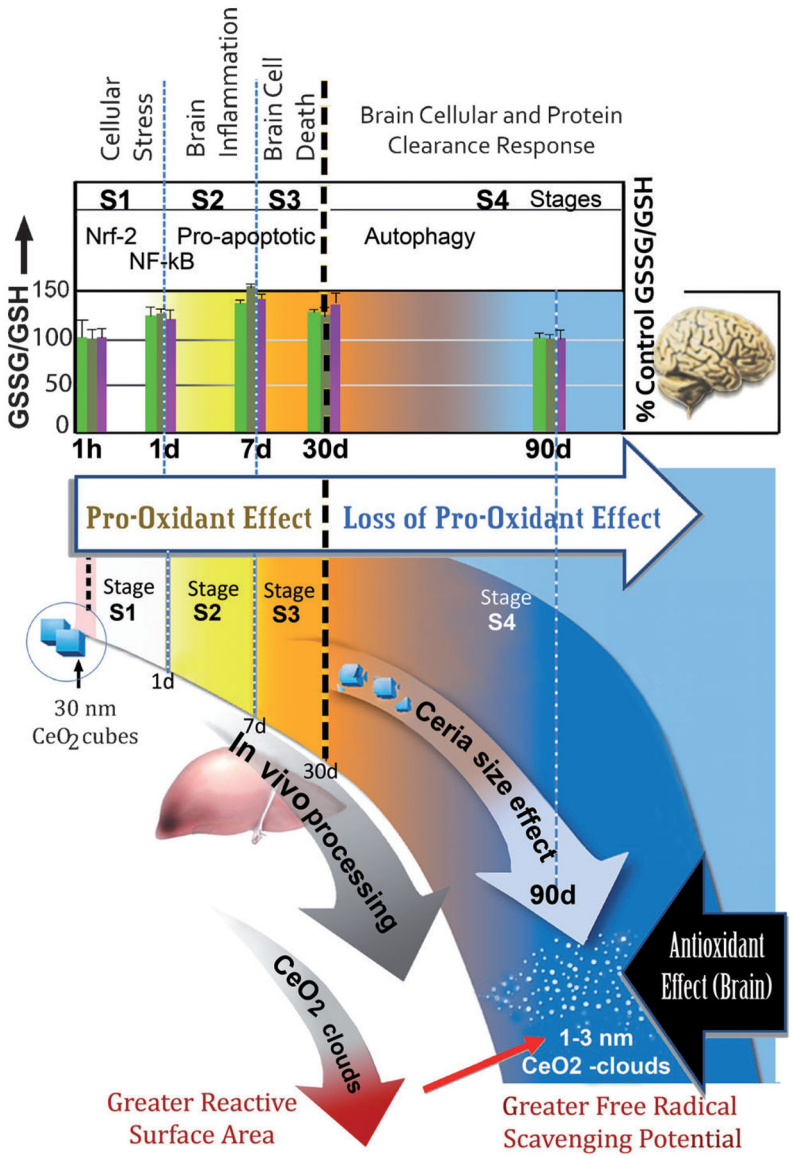

Figure 4.

Predictive in vivo processing model of CeO_2 in the rat liver is shown in temporal relation to brain effects after intravenous administration of 30 nm CeO_2. The top part illustrates signaling pathways (Nrf-2; NF-kB, pro-apoptotic, autophagy) with measured GSSG:GSH from our previous study[21] for three brain regions (neon-green =hippocampus; olive-green = - cortex; purple =cerebellum) taken at different time intervals ranging from 1 h to 90 d. The bottom part illustrates in vivo processing of CeO_2 in the liver during the same time intervals with formation of CeO_2 clouds (second-generation ceria). Four distinct stages (S1–S4) are indicated for both the brain and liver. CeO_2 cloud formation at 90 d coincides with measured loss of the pro-oxidant effect in brain.